Targeting HIF-2α in Colorectal Cancer Reveals a Cholesterol Biosynthesis–Dependent Ferroptotic Vulnerability

Prarthana J. Dalal[1,2*], Rashi Singhal[3*], Boyan Hu[2], Nicholas J. Rossiter[2], Chesta Jain[2], Peter Sajjakulnukit[2], Costas A. Lyssiotis[2], Yatrik M. Shah[2]

[1]University of Michigan, Department of Internal Medicine, Division of Hematology/Oncology, Ann Arbor, Michigan

[2]University of Michigan, Department of Molecular & Integrative Physiology, Ann Arbor, Michigan

[3]Odyssey Therapeutics, Ann Arbor, Michigan

*Both authors contributed equally

Corresponding Author
Yatrik M. Shah, PhD
shahy@umich.edu
7712B Med Sci II
1137 E. Catherine St.
Ann Arbor MI 48109-5622
Telephone: 734-615-0567
Fax: 734-936-8813

Running Title: HIF-2α Inhibition with Statins Decreases Colorectal Carcinoma Growth

Conflict of Interest Disclosure Statement: The authors declare that there are no conflicts of interest regarding the publication of this manuscript.

Abstract:

Colorectal carcinoma (CRC) remains a major cause of cancer-related mortality, with rising incidence in individuals under 55, highlighting the need for novel therapeutic strategies. Hypoxia-inducible factor 2 alpha (HIF-2α) has been genetically validated as a critical driver of colorectal tumorigenesis, with intestinal epithelium–specific deletion in mice markedly reducing tumor formation. While selective HIF-2α inhibitors such as PT2385 are FDA-approved for renal cell carcinoma, pharmacologic HIF-2α inhibition has not been explored in CRC. Here, we demonstrate that HIF-2α inhibition alone fails to suppress CRC growth in vitro under normoxic or hypoxic conditions and in xenograft models in vivo. To identify vulnerabilities induced by HIF-2α blockade, we performed an unbiased CRISPR metabolic screen, revealing cholesterol biosynthesis as a critical dependency. Targeting this pathway with clinically approved statins (atorvastatin, pitavastatin, simvastatin) synergized with PT2385 to suppress CRC cell growth, reduce colony formation, and enhance cell death. Mechanistic studies show that combined HIF-2α and HMG-CoA reductase inhibition promotes ferroptosis, characterized by increased lipid peroxidation and depletion of antioxidant metabolites. These effects are fully reversed by the ferroptosis inhibitor liproxstatin-1. Genetic knockdown of HIF-2α or HMG-CoA reductase recapitulated the enhanced sensitivity to combination therapy. In vivo, co-administration of PT2385 and atorvastatin significantly reduced tumor growth and increased ferroptotic cell death in xenografts, confirming the mechanistic link. Collectively, these findings uncover a metabolic vulnerability of CRC to dual HIF-2α and cholesterol biosynthesis inhibition, supporting a clinically actionable strategy that leverages safe, FDA-approved statins to potentiate HIF-2α-targeted therapy.

Introduction:

Cancer is the second-leading cause of death in the United States and colorectal carcinoma (CRC) is the third most common malignancy [1]. Notably, there is an alarming increase in CRC incidence and mortality among individuals below the age of 55 [2]. This is a demographic in which standard preventive measures such as colonoscopy may fail to detect or eliminate early-stage disease. This highlights the urgent need to expand available therapeutic strategies, particularly for advanced-stage CRC.

CRC is characterized by significant tissue hypoxia arising from the dynamics of countercurrent exchange in blood flow, variations in oxygen demands, altered tumor metabolism, and proximity to an anoxic lumen [3]. Hypoxia inducible factors (HIFs) such as HIF-1α and HIF-2α transcriptionally orchestrate the cellular response to hypoxia and are involved in numerous pathways responsible for cell proliferation, survival, cell death, migration, and metabolism [4].

Specifically, HIF-2α plays a particularly important role in CRC progression. Its expression is elevated in CRC compared with normal colonic epithelium and correlates with reduced disease-free survival [5]. Intestinal epithelium–specific deletion of HIF-2α in mice markedly decreases tumor formation [6]. Mechanistically, HIF-2α promotes colorectal carcinogenesis through recruitment of intratumoral neutrophils [7], dysregulating iron homeostasis [8], potentiating Yes-associated protein 1 (YAP1) activity [9], and in affecting the cyclooxygenase 2 (COX2) / prostaglandin E2 (PGE2) axis [10].

HIF-2α has recently emerged as a therapeutic target with the development of selective small-molecule inhibitors PT2385, a first-in-class, orally available HIF-2α inhibitor. PT2385, the precursor compound, was the first HIF-2α antagonist tested in humans, and led to the development of belzutifan, which was ultimately approved for clinical use [11]. PT2385 blocks HIF-2α dimerization with ARNT (HIF-1β), thereby preventing transcriptional activation of HIF-2α target genes. Renal cell carcinoma (RCC) was prioritized for clinical development because of its unique pathogenesis: von Hippel-Lindau (VHL) tumor suppressor loss drives constitutive HIF-2α accumulation, even under normoxic conditions [12]. Despite this clinical success, HIF-2α inhibition has not been tested in CRC. Given preclinical evidence for HIF-2α's essential role in murine colon tumorigenesis, we hypothesized that HIF-2α inhibition may represent a viable therapeutic strategy in CRC and aimed to uncover specific metabolic vulnerabilities associated with HIF-2α blockade.

Here, we show that HIF-2α inhibition alone does not suppress CRC growth under normoxic or hypoxic conditions in vitro or in vivo. To uncover potential metabolic dependencies, we performed an unbiased CRISPR metabolic screen in CRC cells treated with HIF-2α inhibition. This approach identified cholesterol biosynthesis as a critical vulnerability. Combination therapy with HIF-2α inhibition and 3-hydroxy-3-methylglutaryl-coenzyme A (HMG-CoA) reductase inhibition synergistically suppressed CRC growth and enhanced cell death. HMG-CoA reductase, the rate-limiting enzyme in cholesterol biosynthesis, is the pharmacologic target of statins and are safe and widely prescribed agents for cardiovascular disease [13].

Mechanistically, we demonstrate that the increased cell death observed with combination HIF-2α and HMG-CoA reductase inhibition is mediated by ferroptosis, an iron-dependent form of cell death. Ferroptosis is characterized by an increase in intracellular iron, oxidation of phospholipids containing polyunsaturated fatty acid (PUFAs), and loss of glutathione peroxidase 4 (GPX4) function. Enhancing ferroptosis is emerging as a potent anti-cancer strategy [14].

While novel ferroptosis-inducing agents are under investigation, our findings highlight the potential of repurposing FDA-approved statins in combination with HIF-2α inhibition for CRC therapy.

Results:

HIF-2α inhibition does not affect CRC growth in vitro or in vivo.

As an initial step to assess the therapeutic potential of HIF-2α inhibition in colorectal cancer (CRC), we evaluated whether pharmacological inhibition of HIF-2α with the selective antagonist PT2385 altered CRC growth in vitro. Under normoxic conditions (21% O_2), PT2385 treatment had no effect on the proliferation of HCT116 or SW480 cells relative to vehicle controls (Figure 1A). Because HIF-2α is stabilized under hypoxic conditions, we next hypothesized that reduced oxygen availability might sensitize CRC cells to PT2385. However, even under hypoxia (2% O_2), PT2385 treatment did not alter the growth of either HCT116 or SW480 cells (Figure 1B).

To determine whether these observations extended in vivo, we implanted HCT116 and SW480 cells into immunodeficient nude mice and administered either PT2385 or vehicle daily (Figure 1C). Tumor growth was monitored over a 24-day period, followed by endpoint analyses. In agreement with the in vitro results, PT2385 treatment did not significantly alter tumor growth kinetics (Figure 1D), final tumor volume (Figure 1D), apoptosis as measured by TUNEL staining (Figure 1E), or proliferation as assessed by BrdU incorporation (Figure 1E).

To identify metabolic dependencies that might arise from HIF-2α inhibition, we performed an unbiased CRISPR screen in HCT116 cells using a metabolic gene library (Figure 1F). Gene fitness profiles were compared between vehicle- and PT2385-treated cells. Several genes emerged as key metabolic essentialities in CRC cells treated with HIF-2α inhibition (Figure 1G). This includes phosphatidylinositol 4-kinase beta (PI4KB), mevalonate diphosphate decarboxylase (MVD), and adenosylhomocysteinase (AHCY). Cholesterol biosynthesis genes including sterol regulatory element binding protein cleavage activating protein (SCAP), phosphomevalonate kinase (PMVK), and HMG-CoA reductase (HMCG

Metabolic vulnerabilities of HIF-2α inhibition in colorectal carcinoma

To functionally assess these targets, we tested selective small molecule inhibitors in combination with PT2385. IN-10 is a potent PI4KB inhibitor, however it did not affect HCT116 or SW480 growth when combined with PT2385 (Figure 2A). IN-10, a potent PI4KB inhibitor, did not impact HCT116 or SW480 proliferation in the presence of PT2385 (Figure 2A). Similarly, 6-fluoromevalonate (6FM), an inhibitor of the mevalonate pathway, failed to enhance PT2385 efficacy (Figure 2B). Finally, 3-deazaneplanocin A hydrochloride (DZNep), a dual inhibitor of EZH2 and AHCY, did not significantly affect CRC proliferation in combination with PT2385 (Figure 2C).

Combination HIF-2α inhibition and statins suppress CRC growth

Within the top 30 hits from the CRISPR screen, cholesterol biosynthesis emerged as a recurrent pathway of interest. In addition to MVD, phosphomevalonate kinase (PMVK) and SREBP cleavage-activating protein (SCAP) were identified as essential under conditions of HIF-2α inhibition. To target this pathway in a clinically translatable manner, we employed statins, which inhibit HMG-CoA reductase, the rate-limiting enzyme in cholesterol biosynthesis.

We tested three statins, atorvastatin (Figure 3A), pitavastatin (Figure 3B), and simvastatin (Figure 3C). In both HCT116 and SW480 cells, statins in combination with PT2385 produced a synergistic suppression of growth. Notably, the half-maximal inhibitory concentration (IC_{50}) of simvastatin was significantly reduced when combined with PT2385 compared to simvastatin monotherapy (Figure 3D). A colony formation assay confirmed the long-term impact of combined inhibition. HIF-2α inhibition alone did not alter colony formation, whereas both simvastatin and atorvastatin significantly reduced colony number relative to vehicle controls. This effect was further potentiated by PT2385 (Figure 4C). To determine whether this synergistic growth suppression reflected decreased proliferation or increased cell death, we performed Sytox Green assays. Combination treatment significantly increased the proportion of Sytox Green–positive cells in both HCT116 and SW480, indicating that enhanced cell death underlies the observed effect (Figure 3E).

We next validated these findings using genetic approaches. Validated knockdown of shRNA targeting HIF-2α in HCT116 has been previously published [15]. Western blot for SW480 cells transduced with shRNA targeting HIF-2α is shown in Figure 4A. These SW480 cells exhibited enhanced sensitivity to atorvastatin, pitavastatin, and simvastatin, demonstrating reduced proliferation compared to statin treatment alone (Figure 4B). Conversely, doxycycline-inducible shRNA-mediated knockdown of HMG-CoA reductase was performed in both HCT116 and SW480 cells and validated by qPCR (Figure 4C). This sensitized both cell lines to PT2385, significantly reducing proliferation relative to HMG-CoA reductase knockdown alone (Figure 4D).

HIF-2α inhibition and HMG-CoA reductase inhibition synergize through ferroptosis

To explore the mechanism driving enhanced cell death, we assessed intracellular ferrous iron accumulation using FerroOrange as a readout of ferroptosis. Combined statin and PT2385 treatment modestly increased cytosolic ferrous iron in both HCT116 and SW480 compared to either treatment alone, whereas mitochondrial iron levels measured by Mito-FerroGreen were unchanged (Figure 5A).

We next quantified lipid reactive oxygen species (ROS), another hallmark of ferroptosis. PT2385 plus statin significantly elevated lipid ROS in both HCT116 and SW480 cells, an effect completely abrogated by liproxstatin-1, a selective ferroptosis inhibitor (Figure 5B).

To further investigate the metabolic basis of this ferroptotic response, we conducted LC/MS-based metabolomic profiling in HCT116 cells treated with statin plus either scrambled shRNA or HIF-2α knockdown. Among 119 detected metabolites, 59 were significantly altered ($p < 0.05$; Figure 5C). Key metabolic intermediates linked to oxidative stress regulation—including γ-glutamylcysteine (a glutathione precursor), NAD, NADH, and both oxidized and reduced glutathione—were depleted in the combination group (Figure 5C). These results suggest that HIF-2α inhibition diminishes antioxidant capacity, thereby enhancing susceptibility to lipid peroxidation and ferroptosis.

HIF-2α inhibition and HMG-CoA reductase inhibition decrease tumor growth through ferroptosis potentiation *in vivo*

To validate these findings in vivo, we established xenograft models using HCT116 and SW480 cells and randomized mice into five treatment groups: vehicle, PT2385 alone, atorvastatin alone, PT2385 plus atorvastatin, and PT2385 plus atorvastatin with liproxstatin-1 (Figure 6A). Combination treatment with PT2385 and atorvastatin significantly reduced tumor growth kinetics (Figure 6B) and final tumor volume (Figure 6C) compared with either monotherapy. Importantly, the addition of liproxstatin-1 fully reversed these effects, demonstrating ferroptosis dependence.

Flow cytometry revealed significantly increased proportions of dead cells in tumors treated with PT2385 plus atorvastatin compared to either treatment alone, an effect abolished by liproxstatin-1 (Figure 6D). Similarly, lipid ROS levels were elevated in tumors receiving combination treatment, but this was also reversed by liproxstatin-1 (Figure 6E). Together, these results demonstrate that dual inhibition of HIF-2α and HMG-CoA reductase synergistically suppresses CRC growth in vivo through induction of ferroptosis.

Discussion:

Our study demonstrates that while pharmacologic inhibition of HIF-2α alone does not impair CRC growth, concurrent inhibition of HIF-2α and cholesterol biosynthesis with statins produces a synergistic anti-tumor effect by inducing ferroptosis. This contrasts with renal cell carcinoma (RCC), where HIF-2α inhibition is an established therapeutic strategy, and highlights important tumor type–specific differences in HIF-2α dependency.

We initially expected PT2385, a first-generation selective HIF-2α antagonist, to suppress CRC growth given prior evidence that HIF-2α contributes to colorectal tumorigenesis through altered iron absorption, cancer stem cell–like phenotypes, neutrophil recruitment, and activation of COX2/PGE2 signaling [7-10]. However, PT2385 had no effect on CRC proliferation in vitro or in vivo. One explanation for this discrepancy is that complete genetic loss of HIF-2α during tumor initiation fundamentally alters tumor biology, whereas acute pharmacologic inhibition in established tumors may be insufficient to disrupt redundant or compensatory pathways. In addition, small-molecule antagonists such as PT2385 block HIF-2α/ARNT dimerization but may not fully recapitulate the broad transcriptional and metabolic consequences of HIF-2α deletion. Together, these distinctions suggest that pharmacologic inhibition may unmask context-dependent vulnerabilities rather than phenocopying genetic ablation, leading us to investigate whether HIF-2α inhibition creates exploitable metabolic liabilities.

An unbiased metabolic CRISPR screen identified the cholesterol biosynthesis pathway as a top vulnerability under conditions of HIF-2α inhibition. Functional validation revealed that pharmacologic or genetic inhibition of HMG-CoA reductase synergized with HIF-2α inhibition across multiple CRC cell lines. Importantly, this effect was consistent across several clinically used statins, suggesting a class effect rather than a drug-specific property. Mechanistically, dual inhibition promoted ferroptosis. Combination treatment increased lipid peroxidation and ferroptosis-associated cell death, which was fully reversed by the ferroptosis inhibitor liproxstatin-1. Metabolomic profiling further demonstrated depletion of key antioxidant metabolites, including glutathione intermediates and NAD(H), consistent with impaired redox buffering. These findings align with prior reports that statins decrease GPX4 expression and disrupt isopentenyl pyrophosphate–dependent antioxidant pathways, thereby sensitizing cells to lipid peroxidation [16]. Thus, HIF-2α inhibition appears to lower antioxidant capacity, which cooperates with statin-induced GPX4 suppression to drive ferroptosis.

Interestingly, these findings appear paradoxical in light of our prior work showing that HIF-2α inhibition increases resistance to ferroptosis [8]. This discrepancy may be explained by the metabolic rewiring that occurs under conditions of dual pathway inhibition. Specifically, while HIF-2α inhibition alone decreases lipid peroxidation capacity and thus confers ferroptosis resistance, simultaneous blockade of cholesterol biosynthesis appears to push cells past a metabolic threshold where antioxidant defenses collapse. In this setting, the reduced antioxidant buffering created by HIF-2α inhibition cooperates with statin-induced impairment of GPX4 and isoprenoid metabolism to sensitize cells to ferroptosis. Thus, rather than being contradictory, these results highlight the context-dependent effects of HIF-2α inhibition on ferroptosis, revealing a previously unrecognized metabolic liability that can be unmasked by statins.

Clinically, belzutifan (MK-6482) is the next-generation HIF-2α inhibitor derived from PT2385. Belzutifan is FDA-approved for advanced RCC and is under active investigation in multiple solid tumors [11]. Although we employed PT2385 in this study due to its commercial availability, prior mouse studies have shown that PT2385 and belzutifan display equivalent

efficacy and target engagement [17, 18]. Thus, our findings are directly relevant to belzutifan, which is the clinically actionable compound. Nonetheless, an important limitation is that our work was performed using PT2385 in preclinical CRC models. Future studies employing belzutifan, particularly in combination with statins and in clinically relevant CRC settings, will be essential to confirm translational potential. Our data provide the first evidence that statins may sensitize CRC to HIF-2α inhibition, revealing a synthetic lethal interaction that could be exploited therapeutically. Given the widespread availability, safety, and low cost of statins, this approach could have significant translational potential.

In summary, our work establishes that although HIF-2α inhibition with PT2385 alone is ineffective in CRC, it creates a metabolic dependency on cholesterol biosynthesis that can be leveraged by statins to induce ferroptosis. These findings support further investigation of HIF-2α–statin combinations, particularly with belzutifan, in preclinical and clinical settings as a novel therapeutic strategy for CRC.

Materials and Methods:

Cell Lines and Reagents

HCT116 and SW480 cells (ATCC) were cultured in DMEM (Gibco, Thermo Fisher Scientific) with L-glutamine, D-glucose, and sodium pyruvate, supplemented with 10% heat-inactivated fetal bovine serum (FBS), and 1% antibiotic-antimycotic mix (Invitrogen). Cells were maintained at 37°C and 5% CO_2 in a humidified tissue culture incubator. Hypoxia treatment was performed at 37°C, 2% O_2, and 5% CO_2. IN-10 and DZNep were purchased from MedChemExpress. 6FM was purchased from MilliporeSigma. Atorvastatin, pitavastatin, and simvastatin were purchased from Cayman Chemical Company (Cat # 10493, 15414, 10010344). Sytox Green was purchased from Thermo Fisher Scientific (Cat # S7020). Ferroorange was purchased from Millipore Sigma (Cat # SCT210). MitoFerroGreen was purchased from Millipore Sigma (Cat # SCT262).

Animals and Treatments

All animal procedures were approved by the University of Michigan Institutional Animal Care and Use Committee (IACUC, PRO00011805). Six- to eight-week old male and female immunocompromised nude mice were inoculated with 2 million HCT116 or SW480 cells. Cells were implanted as one tumor into the lower flank, and daily treatments began day 7 after visible tumors appeared. For oral gavage vehicle administered was PEG 400:Kolliphor (7:3). For intraperitoneal injection vehicle administered was sterile saline. PT2385 was given as oral gavage at 30mg/kg in PEG 400:kolliphor (7:3). Atorvastatin was given as oral gavage at 10mg/kg in PEG 400:kolliphor (7:3). Liproxstatin was given as intraperitoneal injection at 10mg/kg in sterile saline. Tumor size was measured with digital calipers. At the endpoint mice were sacrificed, and tumors were excised. Tumor volume was measured, and tissues were prepared for flow cytometry.

Western Blotting

Whole-cell lysates were prepared as previously described [19]. Briefly, cells were lysed in RIPA buffer on ice for 15 minutes, followed by centrifugation at 13,000 rpm for 15 minutes. Supernatants were transferred to a new tube, mixed with 5x Laemmli buffer, and boiled at 95 °C for 5 minutes. Protein samples (30 µg per lane) were separated by SDS-PAGE, transferred onto nitrocellulose membranes and immunoblotted overnight at 4°C. Primary antibodies were used at a dilution of 1:1000. These include HIF-2-alpha antibody (Novus Biological, Cat # NB100-122), Beta-Actin antibody (Protein Tech, Cat # 66009-1), and HMG-CoA Reductase antibody (Santa Cruz, Cat # SC-271595). Horseradish peroxidase-conjugated secondary antibodies were used at a dilution of 1:2000 and immunoblots were developed using Chemidoc imaging system (ChemiDoc, Bio-Rad).

Growth Assays

Adherent cell growth was measured the Cytation 5 Imaging Multi-Mode reader with attached BioSpa (Agilent BioTek). Cells (~500/well) were plated in 96-well plates and allowed to adhere overnight. Baseline images (t_0) were acquired and treatments were applied immediately thereafter. Cell numbers were quantified every 24 hours for 27 hours. Data were normalized to t_0 values. Each condition was measured in triplicate per experiment, with at least two independent experiments performed. Representative growth curves are shown.

CRISPR Screen and Analysis
The human CRISPR metabolic gene knockout library was a gift from David Sabatini (Addgene, 110066) [20]. A total of 75 x 10^6 HCT116 cells were seeded at a density of 5 x 10^5 cells per ml in six-well plates. Each contained 3mL DMEM, 10 µg/ml polybrene, and the CRISPR screen library virus. Viral volume was calculated by infecting target cells at several amounts of virus in the presence of polybrene and counting the number of drug-resistant infected cells after 3 days of selection. Target was to achieve at least 1,000 fold representation of each sgRNA in the library. Spin infection was performed by centrifugation at 1,200 *g* for 45 min at 37 °C. After 24 hours of incubation, the medium was replaced with fresh DMEM. Cells were incubated for an additional 24 hours, after which selection with puromycin (1 µg/mL) was started. After three days of puromycin selection, cells were treated with either DMSO or 10 µM PT-2385. Cells were passaged every 3-4 days and reseeded to maintain the original seeding density. Following 14 doublings, 15 million cells from each condition for genomic DNA isolation using the DNeasy blood and tissue kit (Qiagen), according to the manufacturer's protocol.

sgRNA inserts were PCR amplified with using Takara Ex Taq polymerase, purified, and sequenced on a NextSeq Illumina platform. Sequencing reads were mapped to the sgRNA reference library, allowing only exact matches, and the abundance of each sgRNA was quantified.

For each sgRNA, a differential score was calculated as the log2 fold change in abundance between DMSO- and PT-2385 treated samples. Gene-level differential scores were determined by averaging the scores of all sgRNAs targeting the same gene. The distribution of gene scores was standardized by subtracting the mean from each individual gene score and then dividing by the standard deviation (Z-score). The gene score for each condition was defined as the median log2 fold change in abundance between the PT-2385 and vehicle treated populations for all sgRNAs targeting a particular gene.

Generation of shRNA Cell Lines
Constitutively active genetically modified cell lines were generated using the GIPZ lentiviral shRNA system for human EPAS1 targeting the open reading frame (Horizon). Doxycycline-inducible cell lines were generated using the pLKO.1-Tet On system (Addgene, 21915) [21]. Short hairpin RNA (shRNA) sequences were cloned into pLKO.1-Tet On backbones, sequence validated with Sanger Sequencing (GenScript), and lentivirus was produced through the University of Michigan Vector Core. Cells were transfected with lentiviral particles through spinfection at 900 *g* for 1 hour in the presence of polybrene 10 µg/mL and then incubated at 37 °C. After 24 hours the media was changed and cells were allowed to recover for 24 hours before the addition of puromycin 2 µg/mL to the culture media. Cells were maintained in puromycin until an untreated control well demonstrated 100% cell death.

Flow Cytometry for Sytox Green, FerroOrange, and Mito-FerroGreen
Cells were plated in triplicate in six-well plates and treated as indicated for 16 hours. Prior to analysis, cells were washed three times with HBSS. Mito-FerroGreen (5 µM) and FerroOrange (1µM) working solutions were added. Cells were incubated at 37 °C for 30 minutes. The supernatant was discarded and cells were washed again with HBSS three times. Cells were then processed for flow cytometry analyses.

Lipid ROS Measurement
HCT116 or SW480 cells (1 x 10^6) were seeded in 12-well plates. After adhering overnight at 37°C, cells were treated as indicated for 16 hours. Cells were harvested using PBS-EDTA (5mM) buffer, washed once with HBSS, and incubated in HBSS containing 5 μM C11-BODIPY (Thermo Fisher) for 30 minutes at 37 °C. Cells were pelleted, washed, and resuspended in HBSS. Fluorescence intensity was measured using flow cytometry. A minimum of 20,000 cells were analyzed per condition. Data were analyzed using FlowJo software.

Colony Formation Assay
Cells were plated in biological triplicates in six-well plates at 500 cells per well. Cells were treated as indicated. Media and treatments were replenished every 5 days. Assays were concluded at 14 days by fixing cells in cold 10% buffered formalin for 10 minute and staining with 1% crystal violet and 10% methanol solution for 30 minutes. Colonies were manually counted via a study blinded observer.

Metabolomics
Cells were plated at 1 million cells per well in 6 well plates. After 24 hours, cells were treated as indicated in the figure legends for 24 hours. Cells were then washed once with ice-cold PBS, then incubated with cold 80% methanol on dry ice for 10 minutes. Cells were scraped and the polar metabolite supernatant was collected on dry ice. Protein concentration was determined by processing a parallel well and used for normalization. Cell solutions were lyophilized using a SpeedVac concentrator. Metabolite pellets were resuspended in 50:50 methanol/water mixture for liquid chromatography (LC) – mass spectrometry (MS) analysis.

Samples were analyzed on an Agilent 1290 Infinity II Bio LC ultra-high performance liquid chromatography (UPLC) system consisting of a high-pressure binary pump, multicolumn thermostat, and a temperature controlled multisampler. Data were collected using previously published parameters [22, 23]. After acquisition, metabolomics datasets were processed with MassHunter Quantitative analysis software (B0700) and subsequently imported into Mass Profiler Professional (MPP) for chemometrics analysis.

Each metabolite abundance level in each sample was divided by the median of all abundance levels across samples for comparison and statistics. Statistical significance was determined by a one-way ANOVA with a significance threshold of 0.05. Statistically significant metabolites were identified as those with $p < 0.05$. Data were visualized with a heat map generated by online Morpheus software (https://software.broadinstitute.org/morpheus/).

Statistics
Data are represented as mean ± standard deviation unless otherwise indicated. Data are from 3 independent experiments measured in triplicate unless otherwise stated in the figure legend. Unpaired *t* tests were conducted to assess statistical differences between 2 groups. A *p* value of less than 0.05 was considered statistically significant. All statistical tests were carried out using Prism software (GraphPad) or Excel.

Figure 1. HIF2α inhibition does not alter CRC cell proliferation or tumor growth, but a CRISPR screen reveals specific metabolic dependencies. (A) Proliferation of HCT116 and SW480 colorectal carcinoma cells treated with PT2385 (PT) or vehicle under 21% O_2. Sample size n=3. **(B)** Proliferation of HCT116 and SW480 cells treated with PT2385 or vehicle under 2% O_2. Sample size n=3. **(C)** In vivo treatment schematic **(D)** Tumor growth kinetics and final tumor volumes of HCT116 and SW480 xenografts in immunodeficient nude mice treated with either PT2385 or vehicle. Sample size n=1 with 8 technical replicates shown. **(E)** Quantification of apoptosis (TUNEL staining) and proliferation (BrdU) in harvested tumors. Sample size n=1 with 8 technical replicates shown. **(F)** Schematic of metabolic CRISPR screen in HCT116 cells comparing vehicle and PT2385 treated groups. **(G)** List of top 30 genes identified as well as figure of cholesterol biosynthesis pathway hits highlighted. Sample size n=1.
Data are presented as mean ± SEM.

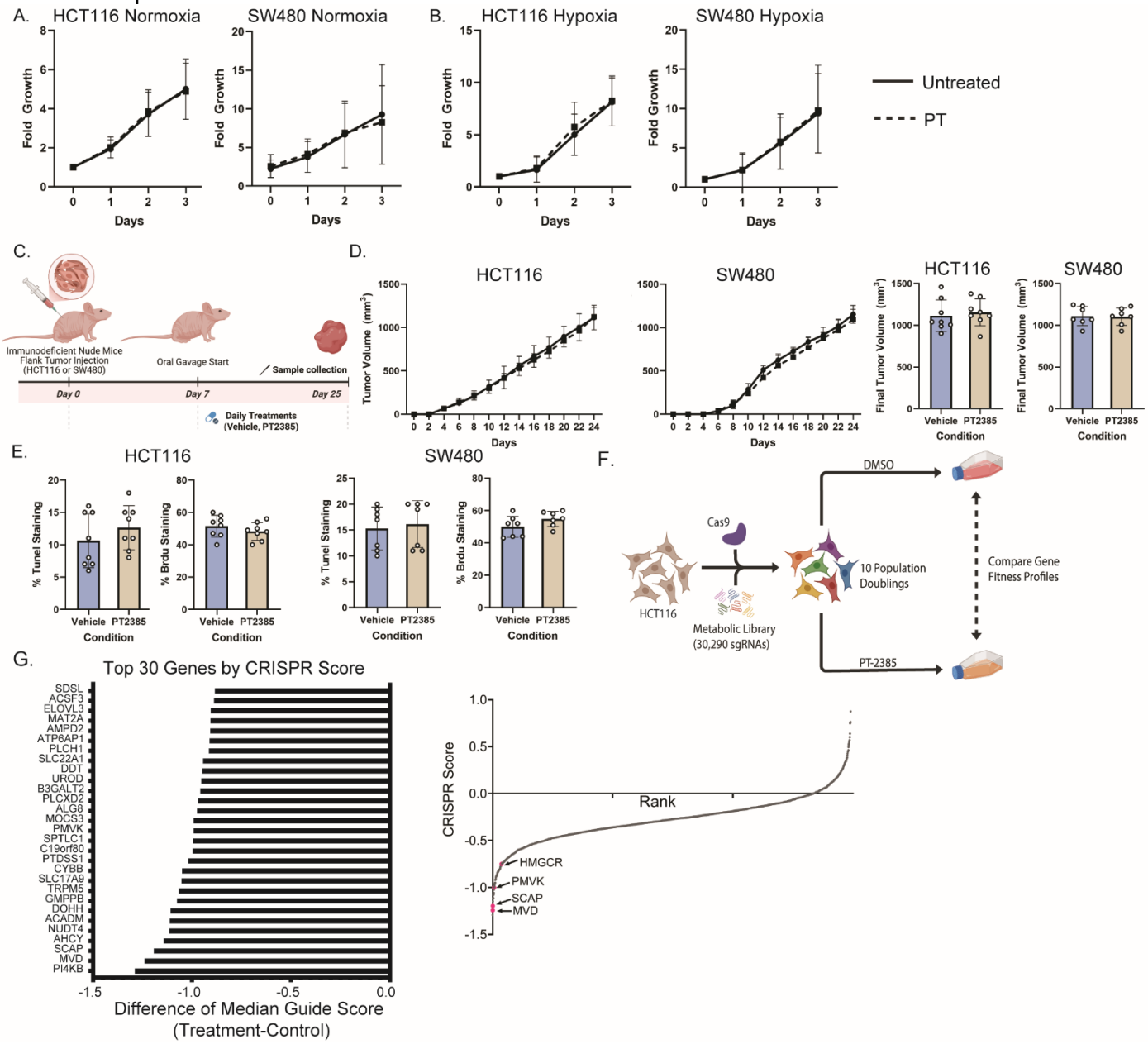

Figure 2. Metabolic vulnerabilities in PI4K, MVD, and AHCY do not sensitize CRC cells to HIF2α inhibition. (A) Proliferation of HCT116 and SW480 cells treated with PI4KB inhibitor IN-10, either alone or in combination with PT2385 (PT). Sample size n=3. **(B)** Proliferation of HCT116 and SW480 cells treated with MVD inhibitor 6-fluoromevalonate (6FM), alone or in combination with PT2385. Sample size n=1. **(C)** Proliferation of HCT116 and SW480 cells treated with dual EZH2 and AHCY inhibitor, 3-deazaneplanocin A hydrochloride (DZNep). Sample size n=2.
Data are presented as mean ± SEM.

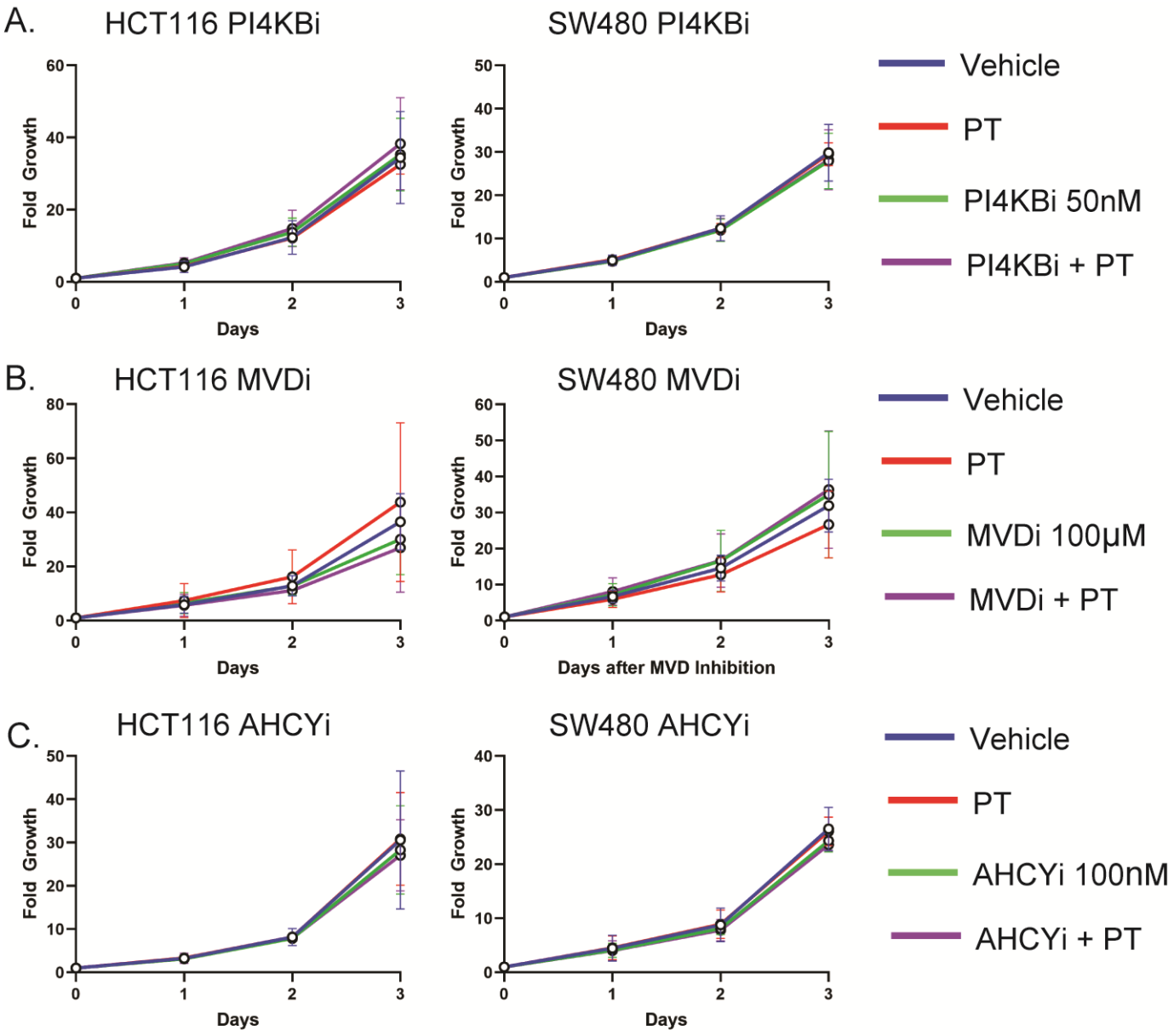

Figure 3. Statins synergize with HIF2α inhibition to suppress CRC cell growth by inducing cell death. (A-C) Proliferation assays in HCT116 and SW480 cells treated with (A) atorvastatin (Atorva), (B), pitavastatin (Pitava), or (C) simvastatin (Simva) either alone or in combination with PT2385 (PT). Sample size n=2 with representative growth curve shown. **(D)** The half maximal inhibitor concentration (IC_{50}) of simvastatin is reduced in the presence of PT2385. Sample size n=1. **(E)** Colony formation assays demonstrate that atorvastatin and simvastatin reduce colony number. This effect is further potentiated with PT2385. Sample size n=1. **(F)** Sytox Green assays quantifying cell death in HCT116 and SW280 cells treated with statin alone or in combination with PT2385 at 24 hours. **(G)** Visual representation of Sytox detected cell death

Data are presented as mean ± SEM; *p<0.05, **p<0.01, ***p<0.001.

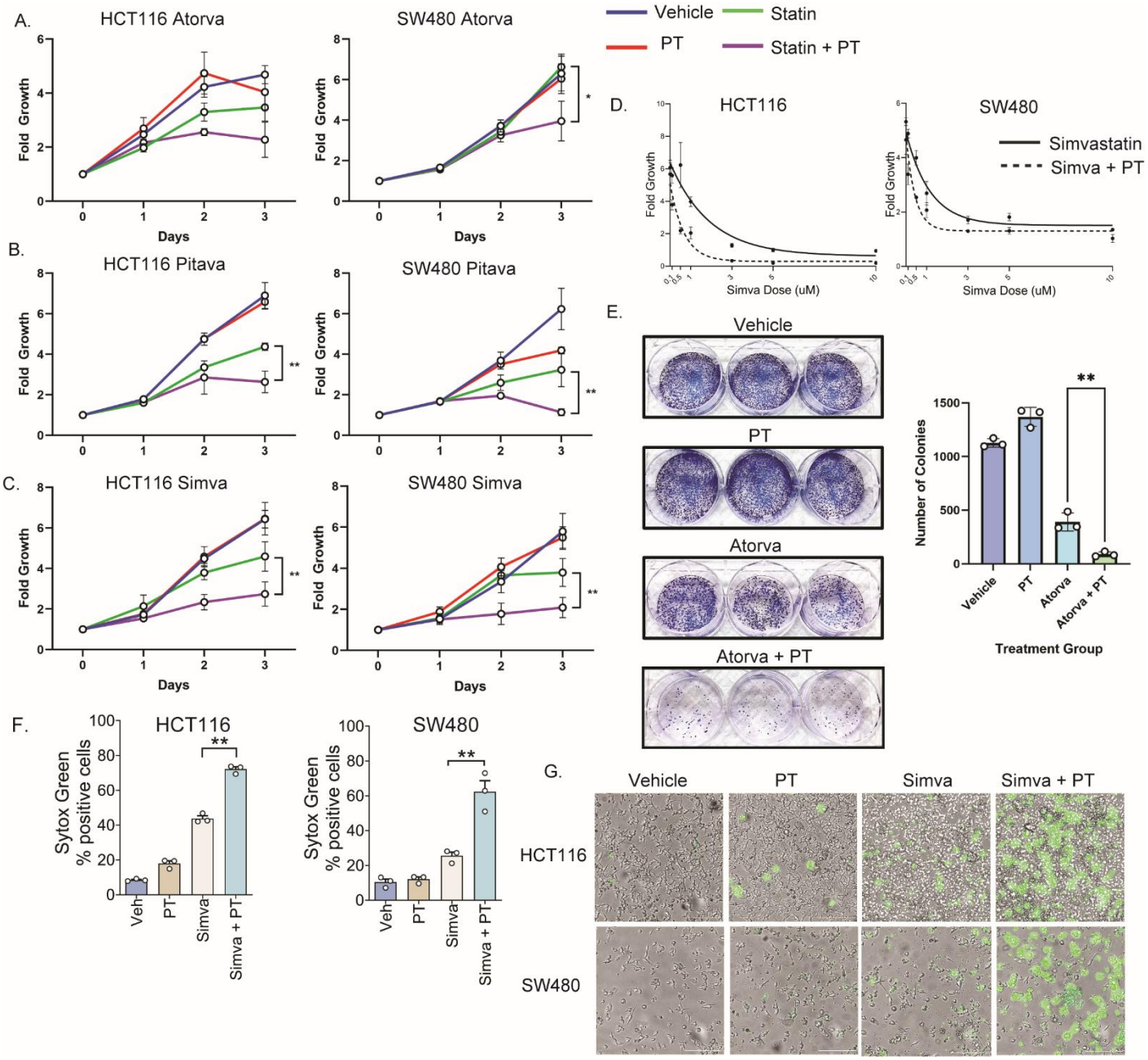

Figure 4. Genetic inhibition of HIF2α and HMG-CoA reductase confirms synergistic suppression of CRC cell proliferation with statin or HIF2α inhibitor treatment respectively. (A) SW480 cells transduced with shRNA targeting HIF2α show significant decrease in HIF2α protein level compared to vehicle. **(B)** HCT116 and SW480 cells transduced with shRNA targeting HIF2α display decreased proliferation when treated with atorvastatin, pitavastatin, or simvastatin. Sample size n=1. **(C)** HCT and SW480 cells transduced with shRNA targeting HMG-CoA reductase (HMGCR) show significant decrease in HMGCR expression by qPCR **(D)** Doxycycline-inducible, shRNA-mediated knockdown of HMG-CoA reductase in HCT116 and SW480 cells decreases cell proliferation when combined with PT2385 (PT) treatment. Sample size n=2 with representative growth curve shown.
Data are presented as mean ± SEM; *p<0.05, **p<0.01, ***p<0.001

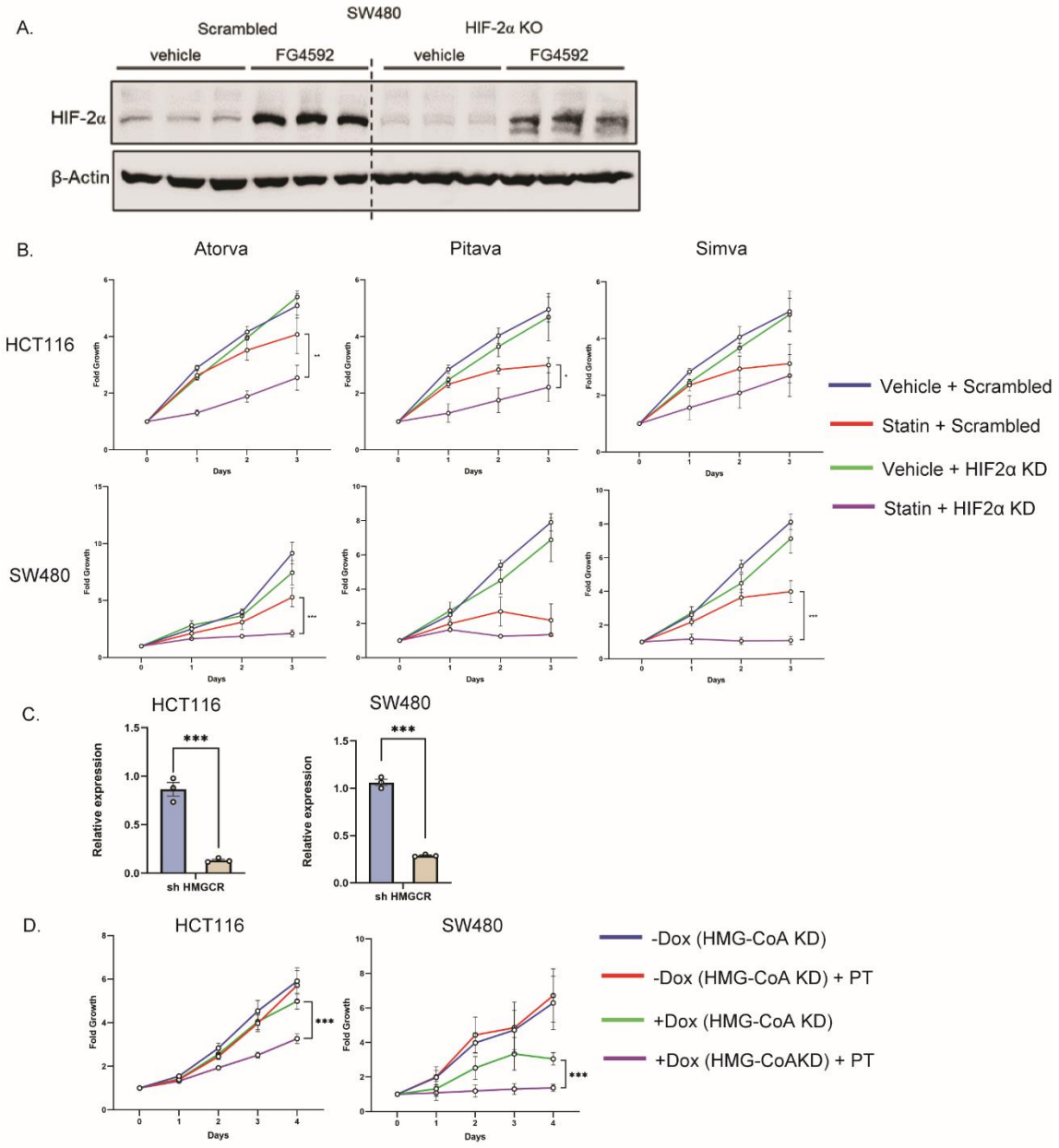

Figure 5. Combined statin and HIF2α inhibition triggers ferroptosis through increased lipid peroxidation and depletion of antioxidant metabolites in CRC cells. (A) Cytosolic ferrous iron levels as measured by FerroOrange trended towards increase in HCT116 and SW480 cells with combined simvastatin (Simva) and PT2385 (PT) treatment compared to either agent alone. Mitochondrial iron levels as measured by MitoFerroGreen remain unchanged. Sample size n=4. **(B)** Combined simva and PT2385 treatment significantly increases lipid ROS. This effect is rescued by the addition of ferroptosis inhibitor liproxstatin-1 (Lip-1) 1μM. Sample size n=1. **(C)** LC/MS metabolomic analysis of HCT116 cells treated with statin plus scrambed vs HIF2α shRNA reveals significant alterations in 59 metabolites. Combination treatment significantly impairs antioxidant capacity as demonstrated by γ-glutamylcysteine, NAD, NADH, reduced glutathione, and oxidative glutathione. Sample size n=1. Data are presented as mean ± SEM; *p<0.05, **p<0.01, ***p<0.001

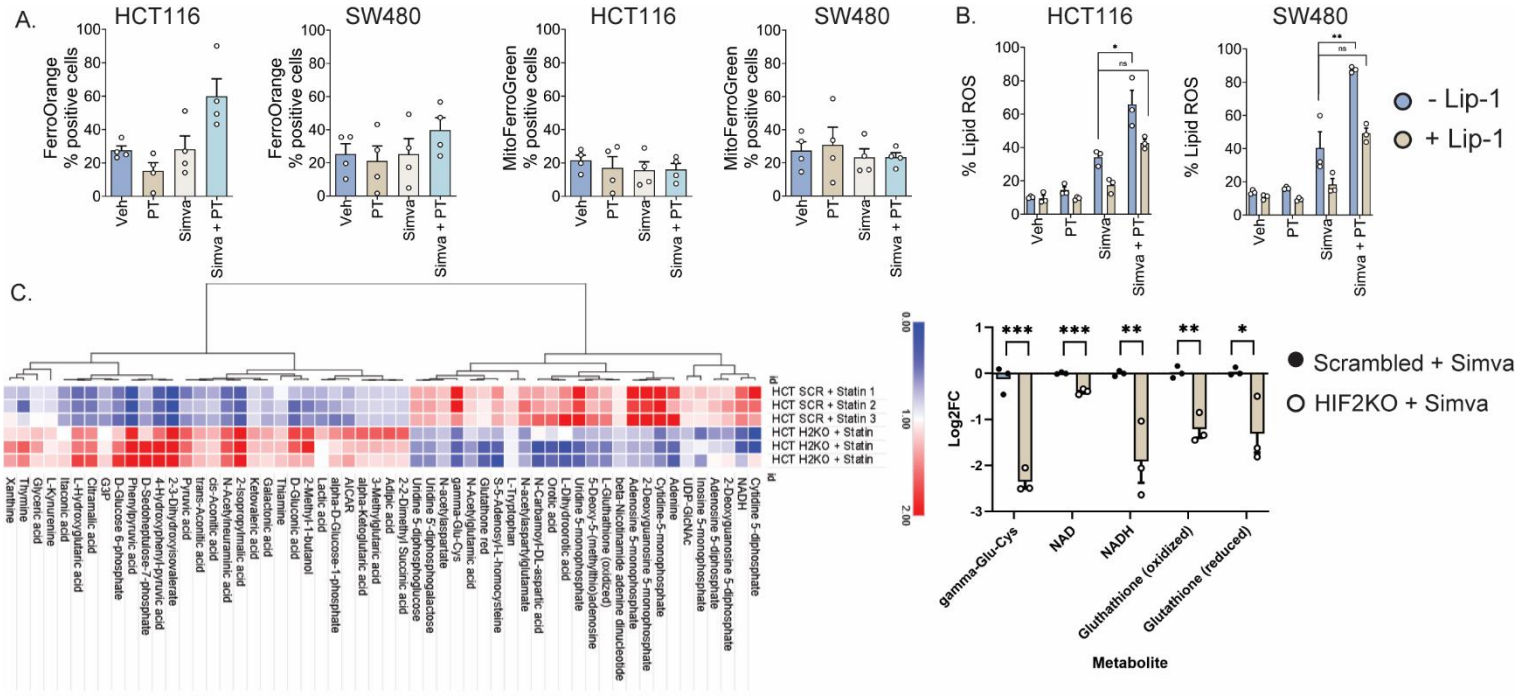

Figure 6. Dual HIF2α and HMG-CoA reductase inhibition with atorvastatin suppresses CRC tumor growth in vivo via ferroptosis-mediated cell death

(A) Experimental design schema **(B)** Tumor growth kinetics in HCT116 and SW480 xenografts treated with vehicle, PT2385, atorvastatin (Atorva), PT2385 (PT) plus atorvastatin, or PT2385 plus atorvastatin and the ferroptosis inhibitor liproxstatin-1. Combination PT2385 and atorvastatin treatment inhibited tumor growth, while liproxstatin-1 reversed this effect. **(C)** Final tumor volumes show marked reduction with PT2385 plus atorvastatin, an effect reversed by liproxstatin-1 co-treatment. **(D)** Flow cytometry shows a significant increase in tumor cell death in the PT2385 plus atorvastatin group, an effect rescued by the addition of liproxstatin-1. **(D)** Lipid reactive oxygen species (ROS) were elevated in tumors treated with PT2385 plus atorvastatin but normalized with the addition of liproxstatin-1 further suggesting ferroptosis-specific cell death.

All data with sample size n=1 presented as mean ± SEM; *p<0.05, **p<0.01, ***p<0.001.

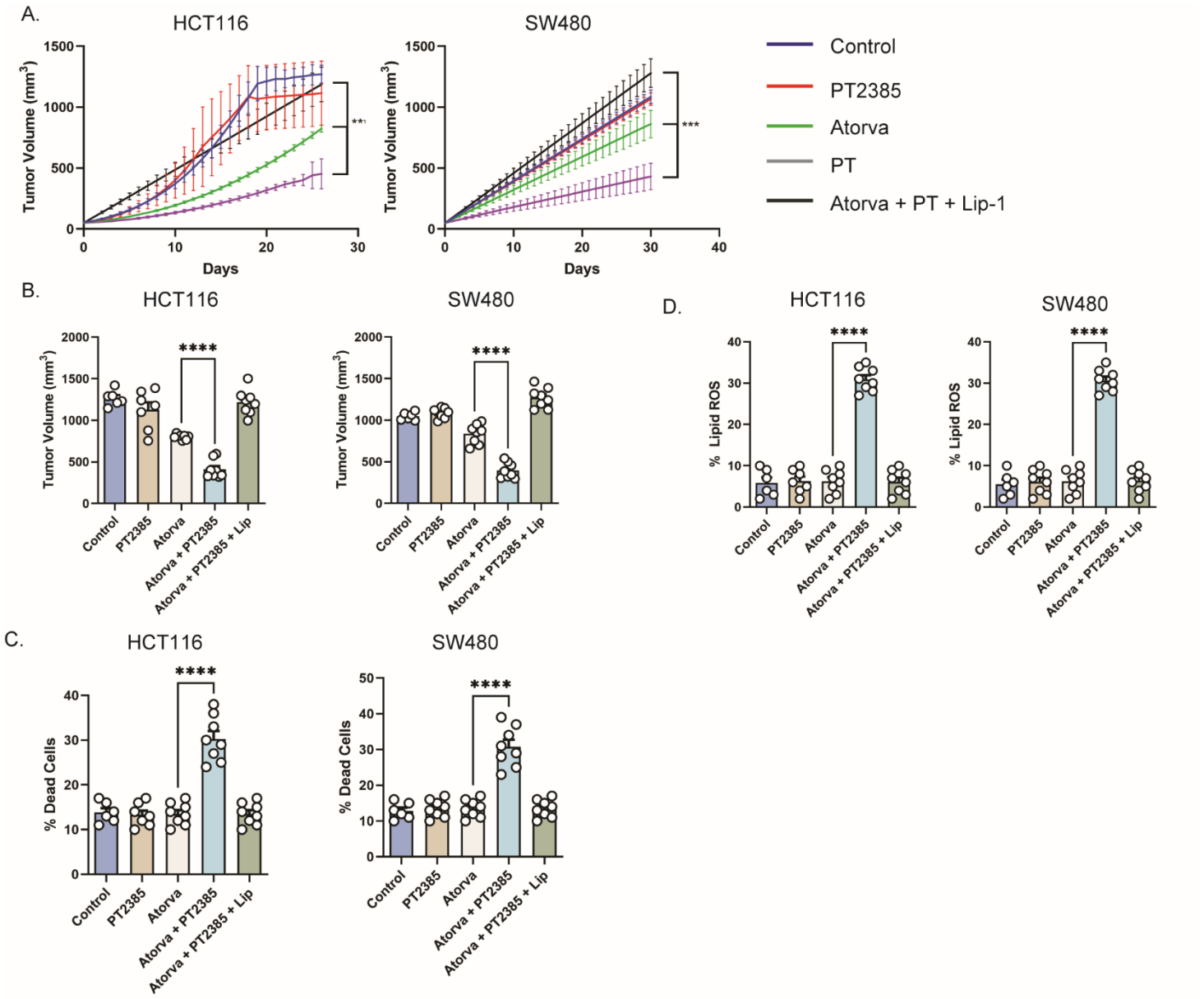

References:

1. Siegel, R.L., T.B. Kratzer, A.N. Giaquinto, H. Sung, and A. Jemal, *Cancer statistics, 2025.* CA Cancer J Clin, 2025. **75**(1): p. 10-45.
2. Shiels, M.S., A.T. Haque, A. Berrington de Gonzalez, M.C. Camargo, M.A. Clarke, B.C. Davis Lynn, E.A. Engels, N.D. Freedman, G.L. Gierach, J.N. Hofmann, R.R. Jones, E. Loftfield, R. Sinha, L.M. Morton, and S.J. Chanock, *Trends in Cancer Incidence and Mortality Rates in Early-Onset and Older-Onset Age Groups in the United States, 2010-2019.* Cancer Discov, 2025: p. OF1-OF14.
3. Singhal, R. and Y.M. Shah, *Oxygen battle in the gut: Hypoxia and hypoxia-inducible factors in metabolic and inflammatory responses in the intestine.* J Biol Chem, 2020. **295**(30): p. 10493-10505.
4. Semenza, G.L., *Hypoxia-inducible factors in physiology and medicine.* Cell, 2012. **148**(3): p. 399-408.
5. Han, S., T. Huang, W. Li, S. Liu, W. Yang, Q. Shi, H. Li, J. Ren, and F. Hou, *Association Between Hypoxia-Inducible Factor-2alpha (HIF-2alpha) Expression and Colorectal Cancer and Its Prognostic Role: a Systematic Analysis.* Cell Physiol Biochem, 2018. **48**(2): p. 516-527.
6. Xue, X., M. Taylor, E. Anderson, C. Hao, A. Qu, J.K. Greenson, E.M. Zimmermann, F.J. Gonzalez, and Y.M. Shah, *Hypoxia-inducible factor-2alpha activation promotes colorectal cancer progression by dysregulating iron homeostasis.* Cancer Res, 2012. **72**(9): p. 2285-93.
7. Triner, D., X. Xue, A.J. Schwartz, I. Jung, J.A. Colacino, and Y.M. Shah, *Epithelial Hypoxia-Inducible Factor 2alpha Facilitates the Progression of Colon Tumors through Recruiting Neutrophils.* Mol Cell Biol, 2017. **37**(5).
8. Singhal, R., S.R. Mitta, N.K. Das, S.A. Kerk, P. Sajjakulnukit, S. Solanki, A. Andren, R. Kumar, K.P. Olive, R. Banerjee, C.A. Lyssiotis, and Y.M. Shah, *HIF-2alpha activation potentiates oxidative cell death in colorectal cancers by increasing cellular iron.* J Clin Invest, 2021. **131**(12).
9. Ma, X., H. Zhang, X. Xue, and Y.M. Shah, *Hypoxia-inducible factor 2alpha (HIF-2alpha) promotes colon cancer growth by potentiating Yes-associated protein 1 (YAP1) activity.* J Biol Chem, 2017. **292**(41): p. 17046-17056.
10. Xue, X. and Y.M. Shah, *Hypoxia-inducible factor-2alpha is essential in activating the COX2/mPGES-1/PGE2 signaling axis in colon cancer.* Carcinogenesis, 2013. **34**(1): p. 163-9.
11. Choueiri, T.K., T. Powles, K. Peltola, G. de Velasco, M. Burotto, C. Suarez, P. Ghatalia, R. Iacovelli, E.T. Lam, E. Verzoni, M. Gumus, W.M. Stadler, C. Kollmannsberger, B. Melichar, B. Venugopal, M. Gross-Goupil, A. Poprach, M. De Santis, F.A. Schutz, S.H. Park, D.A. Nosov, C. Porta, J.L. Lee, X. Garcia-Del-Muro, E. Biscaldi, R. Manneh Kopp, M. Oya, L. He, A. Wang, R.F. Perini, D. Vickery, L. Albiges, B. Rini, and L.-. Investigators, *Belzutifan versus Everolimus for Advanced Renal-Cell Carcinoma.* N Engl J Med, 2024. **391**(8): p. 710-721.
12. Cho, H. and W.G. Kaelin, *Targeting HIF2 in Clear Cell Renal Cell Carcinoma.* Cold Spring Harb Symp Quant Biol, 2016. **81**: p. 113-121.
13. Mills, E.J., P. Wu, G. Chong, I. Ghement, S. Singh, E.A. Akl, O. Eyawo, G. Guyatt, O. Berwanger, and M. Briel, *Efficacy and safety of statin treatment for cardiovascular disease: a network meta-analysis of 170,255 patients from 76 randomized trials.* QJM, 2011. **104**(2): p. 109-24.
14. Huang, W., N. Aabed, and Y.M. Shah, *Reactive Oxygen Species and Ferroptosis at the Nexus of Inflammation and Colon Cancer.* Antioxid Redox Signal, 2023. **39**(7-9): p. 551-568.

15. Bell, H.N., R.J. Rebernick, J. Goyert, R. Singhal, M. Kuljanin, S.A. Kerk, W. Huang, N.K. Das, A. Andren, S. Solanki, S.L. Miller, P.K. Todd, E.R. Fearon, C.A. Lyssiotis, S.P. Gygi, J.D. Mancias, and Y.M. Shah, *Reuterin in the healthy gut microbiome suppresses colorectal cancer growth through altering redox balance.* Cancer Cell, 2022. **40**(2): p. 185-200 e6.
16. Yao, X., R. Xie, Y. Cao, J. Tang, Y. Men, H. Peng, and W. Yang, *Simvastatin induced ferroptosis for triple-negative breast cancer therapy.* J Nanobiotechnology, 2021. **19**(1): p. 311.
17. Cho, H., X. Du, J.P. Rizzi, E. Liberzon, A.A. Chakraborty, W. Gao, I. Carvo, S. Signoretti, R.K. Bruick, J.A. Josey, E.M. Wallace, and W.G. Kaelin, *On-target efficacy of a HIF-2alpha antagonist in preclinical kidney cancer models.* Nature, 2016. **539**(7627): p. 107-111.
18. Chen, W., H. Hill, A. Christie, M.S. Kim, E. Holloman, A. Pavia-Jimenez, F. Homayoun, Y. Ma, N. Patel, P. Yell, G. Hao, Q. Yousuf, A. Joyce, I. Pedrosa, H. Geiger, H. Zhang, J. Chang, K.H. Gardner, R.K. Bruick, C. Reeves, T.H. Hwang, K. Courtney, E. Frenkel, X. Sun, N. Zojwalla, T. Wong, J.P. Rizzi, E.M. Wallace, J.A. Josey, Y. Xie, X.J. Xie, P. Kapur, R.M. McKay, and J. Brugarolas, *Targeting renal cell carcinoma with a HIF-2 antagonist.* Nature, 2016. **539**(7627): p. 112-117.
19. Anderson, E.R., M. Taylor, X. Xue, S.K. Ramakrishnan, A. Martin, L. Xie, B.X. Bredell, S. Gardenghi, S. Rivella, and Y.M. Shah, *Intestinal HIF2alpha promotes tissue-iron accumulation in disorders of iron overload with anemia.* Proc Natl Acad Sci U S A, 2013. **110**(50): p. E4922-30.
20. Birsoy, K., T. Wang, W.W. Chen, E. Freinkman, M. Abu-Remaileh, and D.M. Sabatini, *An Essential Role of the Mitochondrial Electron Transport Chain in Cell Proliferation Is to Enable Aspartate Synthesis.* Cell, 2015. **162**(3): p. 540-51.
21. Wiederschain, D., S. Wee, L. Chen, A. Loo, G. Yang, A. Huang, Y. Chen, G. Caponigro, Y.M. Yao, C. Lengauer, W.R. Sellers, and J.D. Benson, *Single-vector inducible lentiviral RNAi system for oncology target validation.* Cell Cycle, 2009. **8**(3): p. 498-504.
22. Bennett, B.D., J. Yuan, E.H. Kimball, and J.D. Rabinowitz, *Absolute quantitation of intracellular metabolite concentrations by an isotope ratio-based approach.* Nat Protoc, 2008. **3**(8): p. 1299-311.
23. Chae, T.U., W.J. Kim, S. Choi, S.J. Park, and S.Y. Lee, *Metabolic engineering of Escherichia coli for the production of 1,3-diaminopropane, a three carbon diamine.* Sci Rep, 2015. **5**: p. 13040.